Exploring ferroelectric and magnetic properties of Tb-substituted m = 5 layered Aurivillius phase thin films

Ahmad Faraz, Jesus Ricote, Ricardo Jimenez, Tuhin Maity, Michael Schmidt, Nitin Deepak, Saibal Roy, Martyn E. Pemble, and Lynette Keeney

Citation: Journal of Applied Physics **123**, 124101 (2018); doi: 10.1063/1.5009986
View online: https://doi.org/10.1063/1.5009986
View Table of Contents: http://aip.scitation.org/toc/jap/123/12
Published by the American Institute of Physics

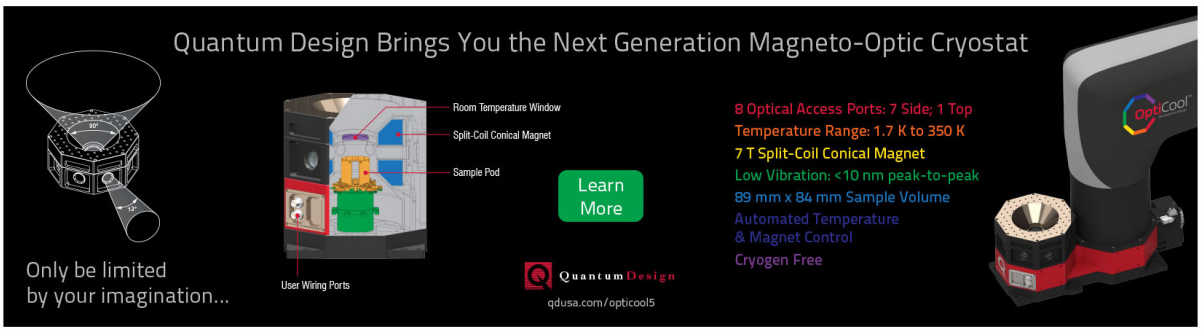

Exploring ferroelectric and magnetic properties of Tb-substituted $m = 5$ layered Aurivillius phase thin films

Ahmad Faraz,[1,a)] Jesus Ricote,[2] Ricardo Jimenez,[2] Tuhin Maity,[1] Michael Schmidt,[1] Nitin Deepak,[3] Saibal Roy,[1] Martyn E. Pemble,[1,4] and Lynette Keeney[1]
[1]*Tyndall National Institute, University College Cork, 'Lee Maltings', Dyke Parade, Cork, Ireland*
[2]*Inst. Ciencia de Materiales de Madrid, CSIC, Cantoblanco, 28049 Madrid, Spain*
[3]*Centre for Materials and Structures, University of Liverpool, Liverpool, United Kingdom*
[4]*Department of Chemistry, University College Cork, Cork, Ireland*

(Received 21 October 2017; accepted 27 February 2018; published online 22 March 2018)

Here, we report the effect of A-site substitution of Tb at the expense of Bi on the ferroelectric and magnetic properties in $m = 5$ layered 2-D Aurivillius $Bi_6Ti_3Fe_2O_{18}$ thin films. The nominal stoichiometry of the prepared compound is $Tb_{0.40}Bi_{5.6}Fe_2Ti_3O_{18}$, $Tb_{0.90}Bi_{5.1}Fe_2Ti_3O_{18}$, and $Bi_6Ti_3Fe_2O_{18}$. Phase examination reveals that only 0.40 mol. % is successfully substituted forming $Tb_{0.40}Bi_{5.6}Fe_2Ti_3O_{18}$ thin films. Lateral and vertical piezoresponse switching loops up to 200 °C reveal responses for $Bi_6Ti_3Fe_2O_{18}$, Tb substituted $Tb_{0.40}Bi_{5.6}Fe_2Ti_3O_{18}$, and $Tb_{0.90}Bi_{5.1}Fe_2Ti_3O_{18}$ thin films along the in-plane (±42.31 pm/V, 88 pm/V and ±134 pm/V, respectively) compared with the out-of-plane (±6.15 pm/V, 19.83 pm/V and ±37.52 pm/V, respectively). The macroscopic in-plane polarization loops reveal in-plane saturation (P_s) and remanence polarization (P_r) for $Bi_6Ti_3Fe_2O_{18}$ of ±26.16 $\mu C/cm^2$ and ±22 $\mu C/cm^2$, whereas, ±32.75 $\mu C/cm^2$ and ±22.11 $\mu C/cm^2$, ±40.30 $\mu C/cm^2$ and ±28.5 $\mu C/cm^2$ for $Tb_{0.40}Bi_{5.6}Fe_2Ti_3O_{18}$ and $Tb_{0.90}Bi_{5.1}Fe_2Ti_3O_{18}$ thin films, respectively. No ferromagnetic signatures were observed for $Bi_6Ti_3Fe_2O_{18}$ and $Tb_{0.40}Bi_{5.6}Fe_2Ti_3O_{18}$. However, a weak response was observed for the $Tb_{0.90}Bi_{5.1}Fe_2Ti_3O_{18}$ at 2 K. Microstructural analysis of $Tb_{0.90}Bi_{5.1}Fe_2Ti_3O_{18}$ revealed that it contains 4 vol. % Fe:Tb rich areas forming $Fe_xTb_yO_z$, which accounts for the observed magnetic moment. This study demonstrates the importance of thorough microstructural analysis when determining whether magnetic signatures can be reliably assigned to the single-phase system. We conclude that $Tb_{0.40}Bi_{5.6}Fe_2Ti_3O_{18}$ and $Tb_{0.90}Bi_{5.1}Fe_2Ti_3O_{18}$ samples are not multiferroic but demonstrate the potential for Fe-RAM applications. *Published by AIP Publishing.*
https://doi.org/10.1063/1.5009986

I. INTRODUCTION

Magnetoelectric materials, demonstrating the coupling of magnetism to electric polarization and vice versa,[1] are of considerable interest from the academic point of view due to the interesting physical phenomena they demonstrate and also because of their commercial potential for use in device applications, e.g., magnetoelectric random access memories (MERAMs),[2] actuators,[3] sensors,[4] etc. Bi-based Aurivillius phase layer structured materials exhibit $(Bi_2O_2)^{2+}$ blocks lying along the (001) plane with alternating perovskite ($nABO_3$) units [general formula $Bi_2O_2(A_{m-1}B_mO_{3m+1})$] and can be viewed as 2-dimensionally layered nanostructures with relatively large c-lattice parameters, in the nanometre (nm) range.[5–9] These materials are considered potential alternatives to lead-based ferroelectric systems due to their attractive physical capabilities such as high Curie temperatures (T_c), the stereo-chemical activity of $6s^2$ lone pair of Bi^{3+} ions (which increases the non-centrosymmetry even more the PZT), and accommodation of different types of cations at the A (1^+–3^+) or B (3^+–5^+) sites of the available perovskite units in consideration of the structural tolerance factor (T_f).[6–8] Due to conflicting competing intrinsic electronic structure requirements, ferroelectricity and ferromagnetism, tend to be mutually exclusive but may be combined in a single-phase material by incorporating both magnetic (partially filled d orbitals) cations and ferroelectric cations (empty d orbitals) within a perovskite-like block of the Aurivillius layer structure.[10] Multiferroic materials are scarce and until recently there are very few materials demonstrating both ferroelectric and ferromagnetic properties in a single-phase. The most extensively studied room temperature multiferroic materials are $BiFeO_3$ (room temperature ferroelectric ($T_c = 110$ K)/($T_N = 643$ K) ferromagnetic) and $BiMnO_3$ [which is a low temperature ($T_c = \sim 105$ K) ferromagnetic oxide reported to be ferroelectric ($T_c = \sim 450$ K)].[11–13] Keeney *et al.*[14] and Faraz *et al.*[15] have recently reported room temperature in-plane ferromagnetic signatures from chemical solution deposition (CSD) and liquid injection chemical vapour deposition (LI-CVD) grown Aurivillius phase $Bi_6Ti_{2.8}Fe_{1.52}Mn_{0.68}O_{18}$ thin films. These materials also demonstrate magnetoelectric multiferroic behaviour where Ti^{4+} cations derive ferroelectricity and magnetic Fe^{3+} and $Mn^{3+/4+}$ cations drive ferromagnetism within the same unit cell. Single-phase multiferroic materials not only have the potential for incorporation into low-power memory devices which can be electrically written and magnetically read, the unique potential for these materials would be their incorporation into future-generation four-state memory devices based on four resistive switching states.[16] The major ferroelectric polarization vector in Aurivillius phase materials lies along

a)ahmad.faraz@tyndall.ie

the in-plane a-axis[17,18] which can be possibly altered, tuned, and derived by odd and even number of perovskite units or blocks and by incorporating various cations at the A-site and B-site of the perovskite unit.[15,17,19] Aurivillius structures with an odd number of perovskite blocks (m) have their spontaneous in-plane polarizations (P_s) along the in-plane axis (a-axis) and possess minor polarisation along the out-of-plane c-axis. On the other hand, structures with an even number of perovskite units (m) also have their major in-plane polarization (P_s) along the a-axis, but demonstrate negligible out-of-plane c-axis polarisation.[18] In-plane spontaneous ferroelectric polarization originates from the tilt and rotation of BO_6 octahedra in the perovskite slab, whereas, odd and even perovskite blocks rotate differently. The apex oxygen in the perovskite unit hybridizes with the Bi of the fluorite-like $(Bi_2O_2)^{2+}$ layers; hence, the BO_6 octahedra receive strain energy from the bismuth oxide slab. In Aurivillius phases with even numbers of perovskite blocks, such strain energy is minimized and relieved, because the adjusted mirror symmetry is perpendicular to the c-axis.[9,20,21] It has been reported that the substitution of the A-site, bismuth with possible alternate rare earth (RE) cations, could alter the ferroelectric behaviour and may also influence the ferromagnetic properties.[22–25] The doping level of rare earth ions is very important to optimize ferromagnetism because the excess of rare earth ions may enter into the B-site and further deteriorate the ferroelectricity and magnetism. The rare-earth ions at the A-site of perovskite blocks effectively suppress the space-modulation spin structure of the Bi base perovskite unit in the Aurivillius structure, hence, contributing to the improvement in ferromagnetism.[26,27] Additionally, bismuth which is volatile at elevated temperature may result in oxygen vacancies and can affect the leakage current and fatigue characteristics.[18,28] Hence, partially substituting Bi^{3+} with a suitable alternative cation in the structure may be an effective approach for improving ferroelectric and ferromagnetic behaviour. It has been reported that by substituting A-site Bi^{3+} with trivalent lanthanide ions, such as Tb^{3+}, Nd^{3+}, Eu^{3+}, Ho^{3+} Gd^{3+}, etc., results in improved ferroelectric properties and fatigue.[29–34] Terbium (Tb^{3+}) when substituted at the expense of Bi^{3+} causes orthorhombic distortion and can reduce oxygen vacancies and improve ferroelectric [decrease ferroelectric Curie temperature (T_c)] and fatigue.[34] It has been reported that $m=3$ $Bi_{3.6}Tb_{0.4}Ti_3O_{12}$ thin films showed larger $2P_r$ and fatigue free behaviour.[35] However, there has been no report on the effect of Tb substitution on the ferroelectric and ferromagnetic properties in magnetic $m=5$ $Bi_6Ti_3Fe_2O_{18}$ thin films.

In this paper, we investigate substitution of Bi with Tb at the A-site of the perovskite unit cell in $m=5$ $Bi_6Ti_3Fe_2O_{18}$ by producing thin films with nominal composition $Tb_{0.40}Bi_{5.6}Fe_2Ti_3O_{18}$ and $Tb_{0.90}Bi_{5.1}Fe_2Ti_3O_{18}$ deposited on (001) oriented sapphire substrates by a chemical solution deposition (CSD) process. Lateral and vertical piezoresponse force switching spectroscopy (SS-PFM) loops were generated on $Bi_6Ti_3Fe_2O_{18}$, $Tb_{0.40}Bi_{5.6}Fe_2Ti3O_{18}$, and $Tb_{0.90}Bi_{5.1}Fe_2Ti_3O_{18}$ thin films at elevated temperatures (up to 200 °C) and at room temperature. The local and macroscopic in-plane and out-of-plane electromechanical switching polarization reversal was explored at room and high temperature with and without in-plane interdigitated electrode (IDE) systems. The switching polarization reversal loops demonstrate that $Bi_6Ti_3Fe_2O_{18}$, $Tb_{0.40}Bi_{5.6}Fe_2Ti_3O_{18}$, and $Tb_{0.90}Bi_{5.1}Fe_2Ti_3O_{18}$ thin films are ferroelectric having the potential for use in commercial applications such as high temperature ferroelectric memory and sensor technologies. Ferromagnetic responses were analysed using high resolution magnetic (SQUID) measurements. The prospect of the magnetic responses being intrinsic to the main Aurivillius phase was assessed carefully by analysis of the samples for traces of magnetic impurity phases using X-ray diffraction (XRD), scanning electron microscopy with energy dispersive X-ray spectroscopy (EDX), and high resolution transmission electron microscopy (HR-TEM) and the results are discussed.

II. METHODS

$Bi_6Ti_3Fe_2O_{18}$ and Tb substituted $Tb_{0.40}Bi_{5.6}Fe_2Ti_3O_{18}$ and $Tb_{0.90}Bi_{5.1}Fe_2Ti_3O_{18}$ Aurivillius phase thin films with 5 perovskite layers per half unit cells were synthesized using a chemical solution deposition (CSD) process. Two different sets of samples were prepared. In the first set, we have prepared $m=5$ $Bi_6Ti_3Fe_2O_{18}$ thin films and confirm the percent of Bi excess required to form single-phase $m=5$ $Bi_6Ti_3Fe_2O_{18}$ thin films. Since Bi is volatile at higher temperatures and to suppress the possible formation of pyrochlore phases during the annealing step, to compensate for Bi loss, an additional 0%–15% molar excess of Bi was investigated.[9,36] We systematically studied and found that 10% Bi excess was sufficient to allow and form a 5 layer Aurivillius phase without the formation of pyrochlore phases. Using this information, thin film samples substituted with Tb at the A-site: $Tb_{0.40}Bi_{5.6}Fe_2Ti_3O_{18}$ and $Tb_{0.90}Bi_{5.1}Fe_2Ti_3O_{18}$ were prepared by incorporating or substituting $Tb^{3+}/^{4+}$ in the place of Bi^{3+} in $Bi_6Ti_3Fe_2O_{18}$. $Tb_{0.40}Bi_{5.6}Fe_2Ti_3O_{18}$ and $Tb_{0.90}Bi_{5.1}Fe_2Ti_3O_{18}$ thin film synthesis involves the preparation of two different solutions, namely A and B. Solution A was prepared by dissolving the desired stoichiometric ratio of $Tb(CH_3CO_2)_3{\cdot}xH_2O$ and $Bi(NO_3)_3{\cdot}5H_2O$ in lactic acid at room temperature. While in solution B, Fe $(NO_3)_3{\cdot}9H_2O$, at the appropriate ratio, was dissolved separately in acetyl acetone. After achieving complete dissolution, the Fe^{3+} solution B was slowly introduced into the $Bi^{3+}/Tb^{3+}/^{4+}/Ti^{4+}$ solution A, drop-wise under constant stirring to achieve a 0.03 mol dm^{-3} solution. The film was spin coated onto 2″ C-M plane (0001) oriented, 430 μm thick, single side polished sapphire substrates using a commercially available spin coater (spin coater KW-4A, Chemat Technology) operating at 1000 rpm for 30 s. In the pre-annealing step, the impurities in the form of organic residue and solvents were removed by baking the deposited film on a hot plate at 300 ± 5 °C for roughly 10 min yielding films with an approximate thickness of $100 + 30$ nm, as observed from the cross-section SEM analysis. The films were annealed at 850 °C for 30 min in ambient air in a conventional furnace. The steps involved in the synthesis of Tb-substituted $Bi_4Ti_3O_{12}$-($BiFeO_3$) are represented by the flowchart represented by Fig. 1(a). Please note that same steps were used for the preparation of $Bi_6Ti_3Fe_2O_{18}$ thin films, the only specific molar ratio of $Bi(NO_3)_3{\cdot}5H_2O$

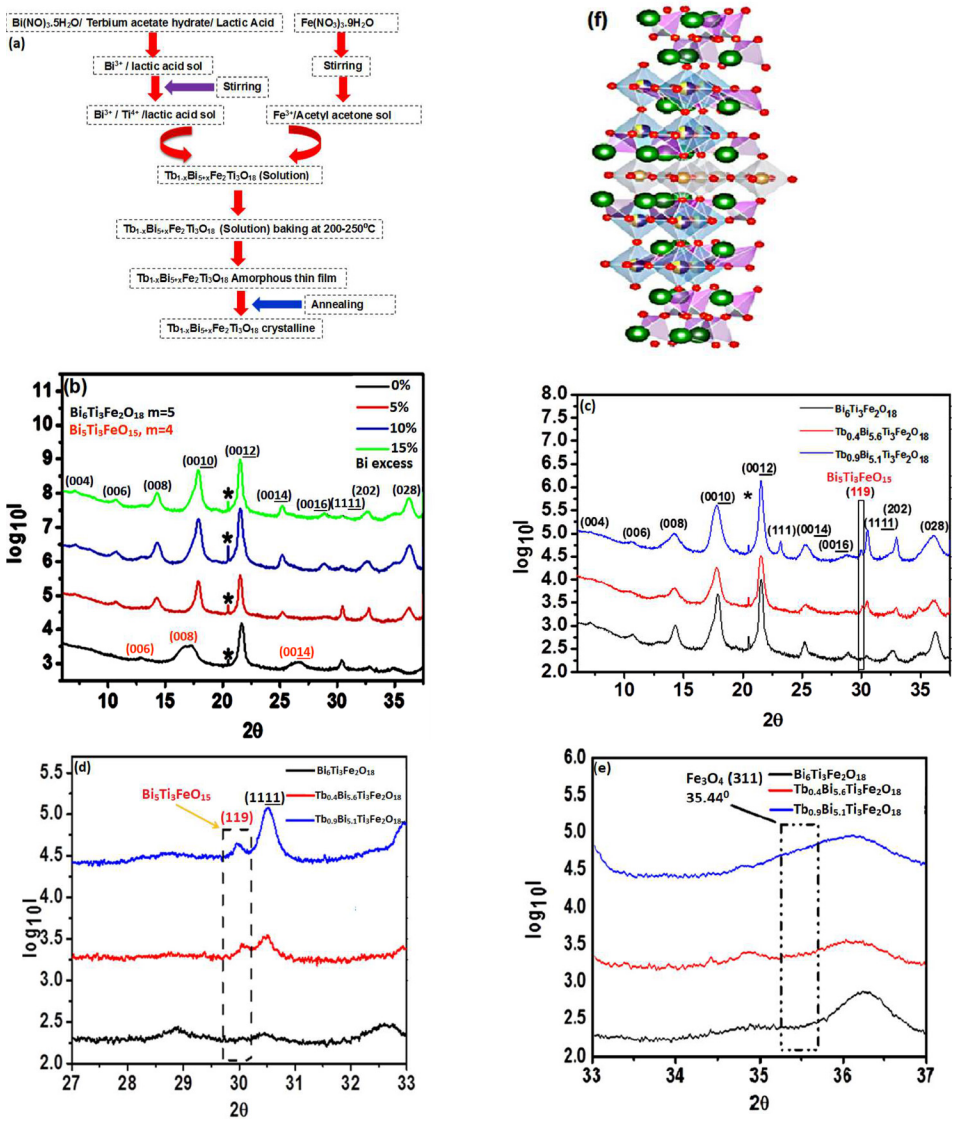

FIG. 1. (a) Chemical solution deposition (CSD) flow sheet demonstrating the synthesis of $Tb_{1-x}Bi_{5+x}Fe_2Ti_3O_{18}$ thin films; X-Ray diffraction (XRD) patterns (b) illustrating the possible % (0%, 5%, 10%, and 15%) of Bi excess required to synthesize single phase $Bi_6Fe_2Ti_3O_{18}$ (it should be noted that these samples were annealed for 30 min at 850 °C); (c) the diffraction patterns from $Bi_6Fe_2Ti_3O_{18}$, $Tb_{0.40}Bi_{5.6}Fe_2Ti_3O_{18}$, and $Tb_{0.9}Bi_{5.1}Fe_2Ti_6O_{18}$ thin films on sapphire substrates (10% excess bismuth was used during the synthetic process); (d) restricted range slow speed scans through the 2-theta region which would be expected to reveal the appearance of secondary $Bi_5FeTi_3O_{15}$ phase (119) reflection on increase in Tb substitution; (e) the presence of the ferromagnetic spinel impurity phases Fe_3O_4 or $TbFe_2O_4$, if present in $Bi_6Fe_2Ti_3O_{18}$, $Tb_{0.40}Bi_{5.6}Fe_2Ti_3O_{18}$, and $Tb_{0.9}Bi_{5.1}Fe_2Ti_6O_{18}$ thin films; (f) the crystal structure of the $m = 5$ Aurivillius phase $Tb_{1-x}Bi_{5+x}Fe_2Ti_3O_{18}$ along the ⟨110⟩ direction with five perovskite units sandwiched between two bismuth oxide blocks.

was used in solution A, with no $Tb(CH_3CO_2)_3{\cdot}xH_2O$. 90:10 nm thick Au: Ti interdigitated electrodes (IDEs) deposited onto 100 ± 30 nm thick $Bi_6Ti_3Fe_2O_{18}$, $Tb_{0.40}Bi_{5.6}Fe_2Ti_3O_{18}$, and $Tb_{0.90}Bi_{5.1}Fe_2Ti_3O_{18}$ thin films using standard optical ultra violet photolithography (UV-photolithography) as illustrated in Figs. 5(c) and 5(d). A Philips Xpert PW3719 MPD X-Ray diffractometer equipped with a CuKα radiation source (operating at 45 kV and 40 mA) and nickel filter, with an incident beam filtered with an X-Ray mirror and the diffracted beam filtered using a monochromator, was used to collect X-Ray diffraction (XRD) patterns over the range $5 \leq 2\theta \leq 37.5^\circ$ at room temperature. The crystallographic orientation (Lotgering factor L_f) was investigated by comparing the ratios of intensities of peaks along the preferred orientation to the summation of all diffracted peak intensities and using theoretical (hkl) intensities obtained from the Crystallographica software.[37,38] High-resolution FEI 630 scanning electron microscopy (HR-SEM) with energy dispersive X-ray spectroscopy (EDX) equipped with a X-Max 20 detector and Inca analysis software and commercially available atomic force microscopy [Asylum Research (AR) AFM MFP-3DTM] were used to conduct morphological and compositional analysis. The surface roughness and topography were analysed using the commercially available MFP-3D TM [Asylum Research (AR)] atomic force microscope (AFM) in the non-contact AC mode, equipped with silicon cantilevers (Olympus AC160TS) (Al reflective coating, 70 kHz electrilever resonance frequency). The $m = 5$ layer structure and a thorough investigation of possible intergrowths of different m phases or other secondary or impurity phases were investigated using high resolution transmission electron microscopy (HR-TEM Jeol; 2100 TEM, 200 kV; double tilt holder). FEI Dual Beam Helios NanoLab 600i Focused Ion Beam (FIB) (final thinning @ 93 pA, 30 kV, final polish 2 kV, 28 pA) was used to prepare cross-sections of the $Bi_6Ti_3Fe_2O_{18}$, $Tb_{0.40}Bi_{5.6}Fe_2Ti_3O_{18}$, and $Tb_{0.90}Bi_{5.1}Fe_2Ti_3O_{18}$ thin films, whereas gold coating was used to prevent surface charging. The major in-plane ferroelectric polarization was explored locally by rastering the PFM tip on the sample in a single-frequency mode (SPFM), with a frequency (20 kHz) lower than the tip resonance (70 kHz) and the tip/sample contact resonance frequency (300–310 kHz). Ferroelectric switching polarization reversal loops were locally generated in dual AC resonance switching spectroscopy (DART-SS PFM) and

lateral single-frequency modes using a triangular step wave form comprised of pulsed DC biases (15 V–50 V) and an AC signal of 5.5 V, and a cycling frequency of 0.2 Hz. In-plane switching ferroelectric polarization was explored macroscopically by generating in-plane switching polarization reversal using IDE architectures deposited on these films and were analysed via a LCCII ferroelectric tester. High resolution magnetic measurements were performed with a superconducting quantum interference device (SQUID Model-MPMS XL5, Quantum Design) magnetometer under a maximum field of 5 T and at a temperature range of 2 K. To ensure that there is no trapped flux both in the superconducting coil of the SQUID and in the sample, a well-designed protocol was followed to demagnetize them.[39]

III. RESULTS AND DISCUSSION

Two different sets of X-ray diffraction (XRD) experiments were performed. In the first set [Fig. 1(b)], XRD was performed on the samples different exhibiting Bi excesses, varied from 0% to 15% (required in order to allow the structure to form $m=5$ layers Aurivillius phase $Bi_6Ti_3Fe_2O_{18}$ without any intergrowths of over m phases) which were annealed at 850 °C for 30 min. The diffraction patterns were highlighted and minor secondary impurity phases were made more visible by plotting in a logarithmic scale. The % of Bi excess is represented by legends with different colours in Fig. 1(b). Peaks designated with an asterisk (*) are from the sapphire substrate and the XRD sample holder. Starting with 0% Bi excess, interesting features are visible in the XRD plots. It can be observed that the samples with 0% Bi excess exhibit mixed $m=4$ ($Bi_5Ti_3FeO_{15}$) and $m=5$ ($Bi_6Ti_3Fe_2O_{18}$) phases. (006), (008), and (0014) reflection peaks were generated from a secondary phase $m=4$ $Bi_5Ti_3FeO_{14}$ layered structure. These secondary phase impurities in Bi-based Aurivillius materials are common because of the volatile nature of Bi at the relatively high annealing temperature used.[9,36] However, to compensate bismuth loss and to allow for a single-phase $m=5$ structure, a sufficiently excess of Bi results in the suppression of secondary impurity phases.[21] We observed from the XRD spectra that $Bi_6Ti_3Fe_2O_{18}$ thin films with 10% Bi excess [Fig. 1(b)] are consistent with the $m=5$ layer Aurivillius phase structure (having 5 perovskite blocks per half unit cell) exhibiting no secondary impurity phases and better crystallinity. The second set of X-ray diffraction (XRD) experiments was performed on $Tb_{0.40}Bi_{5.6}Fe_2Ti_3O_{18}$ and $Tb_{0.90}Bi_{5.1}Fe_2Ti_3O_{18}$ thin film samples as illustrated in Fig. 1(c). An introduction of Tb during the film growth, leads to an interesting diffraction feature in the XRD patterns. First, the (008), (0010), (0012), and (028) diffraction peaks start broadening. The FWHM values for the diffraction planes (008), (0010), (0012), and (028) increase (0.19°, 0.29°, 0.19°–0.22°, 0.17°–0.23°, 0.21°, and –0.34°) with an increase in Tb substitution confirming that the crystallinity decreases with increases in Tb substitution. The effect of Tb substitution on the crystalline quality is investigated by calculating the relative crystalline quality factor parameter, Q, defined as $Q=1/B\cos\theta$, where B is the diffraction peak width (FWHM) in radians and θ is the incident x-ray beam angle (the Q values are illustrated in Table I. These Q factor values were measured by average the values over the prominent ((006), (008), (0010), (0012), and (028) diffraction peaks. It is observed that the crystalline quality (Q) decreases (333–239) with the increase in Tb substitution. XRD patterns reveal that the reflections are consistent with an $m=5$ layered Aurivillius phase structure (having 5 perovskite blocks per half unit cell). The degree of preferred crystallographic orientation, Lotgering factor (L_f) (the values are listed in Table I), was calculated by comparing the ratios of intensities of the peaks along the preferred orientation (00l) to summation of all diffracted intensity peaks and using theoretical *(hkl)* intensities obtained from the Crystallographica software[37,38] confirming that these films are *c*-axis oriented [exhibiting Lotgering factors (L_f) of 0.98, 0.95, and 0.92 for $Bi_6Ti_3Fe_2O_{18}$, $Tb_{0.40}Bi_{5.6}Fe_2Ti_3O_{18}$, and $Tb_{0.9}Bi_{5.1}Ti_3Fe_2O_{18}$ thin films, respectively]. However, on closer look at XRD patterns [Fig. 1(c)] , we observed an additional (119) reflection peak from secondary impurity phase $m=4$ layer $Bi_5FeTi_3O_{15}$. The presence of (119) peak reflection from secondary impurity phase $Bi_5FeTi_3O_{15}$ was thoroughly investigated using slow x-ray diffraction (XRD) with a scan rate of 0.15°/min and a step size of 0.0025° [Fig. 1(d)], performed in the range $27^\circ \leq 2\Theta \leq 33^\circ$. The data analysis suggest that (119) reflection peaks appear on the substitution of Tb in B6TFO films, such as, the B6TFO film with no Tb is purely $m=5$ layer. Furthermore, the intensity of (119) diffraction peaks increases with increase in the Tb volume. The background noise during the x-ray scan limits the detectability of the minor impurity or defects phases to 3 vol. % of the parent phase. Common minor secondary phases detected in Aurivillius phase materials are ferroelectric pyrochlore ($Bi_2Ti_2O_7$) [(222) and (444) reflections at 14.9° and 30°], and ferromagnetic spinel Fe_3O_4 [(311) at 35.4°)] structures. The presence of a small magnetic phase like spinel Fe_3O_4 [(311) at 35.4°)] at trace levels below detectable by XRD could

TABLE I. Comprehensive comparison of crystallographic quality (Q), crystallographic orientation (Lf), and local and macroscopic ferroelectric properties of $Bi_6Ti_3Fe_2O_{18}$, $Tb_{0.40}Bi_{5.6}Fe_2Ti_3O_{18}$, and $Tb_{0.9}Bi_{5.1}Ti_3Fe_2O_{18}$ thin films.

	Q	L_f	Out-of-plane piezoremanence (pm/V)	Out-of-plane piezosaturation response (pm/V)	In-plane piezoremanence P_{rx} (pm/V)	In-plane piezosaturation (pm/V)	Ferroelectric in-plane remanence polarization P_{rx} ($\mu C/cm^2$)	Ferroelectric in-plane saturation polarization P_{sx} ($\mu C/cm^2$)
$Bi_6Ti_3Fe_2O_{18}$	239	0.98	±6.19	±7.55	±37	±47	±22	±26.16
$Tb_{0.4}Bi_{5.6}Ti_3Fe_2O_{18}$	265	0.95	±17	±20	±73	±92	±22.11	±32.75
$Tb_{0.9}Bi_{5.1}Ti3Fe_2O_{18}$	333	0.92	±31	±35	±102	±135	±28.5	±40.30

influence the magnetic properties of a sample.[14,15,40] The slow x-rays scan in the range $33° \leq 2\theta \leq 37°$ [Fig. 1(e)] do not demonstrate obvious spinel Fe_3O_4 [(311) at 35.4°)] peaks, however, the (028) peak which is in close proximity may be masking its signal. It should be noted that the goal of this work was to present a comparison of Tb substituted and $Tb_{0.90}Bi_{5.1}Fe_2Ti_3O_{18}$ with $Bi_6Ti_3Fe_2O_{18}$ thin films. Hence, further experimental work is briefly based on the comparison of physical properties of Tb substituted $Tb_{0.40}Bi_{5.6}Fe_2Ti_3O_{18}$ and $Tb_{0.90}Bi_{5.1}Fe_2Ti_3O_{18}$ with $Bi_6Ti_3Fe_2O_{18}$ thin films. High resolution scanning electron microscopy (HR-SEM) analysis reveals that Tb substituted rate = 500 μs on 5 different areas (scan resolution = 1365×) reveals that the average chemical stoichiometric composition of these films is $Bi_6Ti_3Fe_2O_{18}$, $Tb_{0.40}Bi_{5.6}Fe_2Ti_3O_{18}$, and $Tb_{0.90}Bi_{5.1}Fe_2Ti_3O_{18}$. It should be noted that according to the first principle theory, the origin of ferroelectricity in Bi-based perovskite like $BiFeO_3$ is mainly associated with $6s^2$ lone pair electrons.[41] However, chemical substitution of Bi^{3+} like cations such as rare earth cations (RE) e.g., Tb, is recommended because these effectively improve the ferroelectric and insulating properties of Bi based Aurivillius phase materials. The rare earth (Tb^{3+}, Sr^{3+}, La^{3+}, etc.) cations compensate the volatile Bi component and suppress the formation of oxygen vacancies.[42,43] The structure of Aurivillius phase $m = 5$ layers $Tb_{1-x}Bi_{5+x}$ Ti3Fe_2O_{18} systems is schematically illustrated in Fig. 1(f). $Tb_{0.40}Bi_{5.6}Fe_2Ti_3O_{18}$, $Tb_{0.90}Bi_{5.1}Fe_2Ti_3O_{18}$, and $Bi_6Ti_3Fe_2O_{18}$ thin films exhibit randomly oriented crystallized grains with plate-like morphologies which is characteristic of Aurivillius phase materials [Figs. 2(a)–2(c)]. SEM-EDX analysis (over 50×50 μm^2 performed 5 scans (scan rate- = 500 μs) on 5 different areas (scan resolution = 1365×) reveal that the average chemical stoichiometric composition of these films is $Bi_6Ti_3Fe_2O_{18}$, $Tb_{0.40}Bi_{5.6}Fe_2Ti_3O_{18}$, and $Tb_{0.90}Bi_{5.1}Fe_2Ti_3O_{18}$. It should be noted that according to the first principle theory, the origin of ferroelectricity in Bi-based perovskite like $BiFeO_3$ is mainly associated with $6s^2$ lone pair electrons.[41] However, chemical substitution of Bi^{3+} like cations such as rare earth cations (RE) e.g., Tb, are recommended because these effectively improve the ferroelectric and insulating properties of Bi based Aurivillius phase materials. The rare earth (Tb^{3+}, Sr^{3+}, La^{3+}, etc.) cations compensate the volatile Bi component and suppress the formation of oxygen vacancies.[42,43] This effect of A-site Tb substitution on ferroelectricity can be visualized by investigating and comparing the microscopic and macroscopic ferroelectric properties of $Tb_{0.40}Bi_{5.6}Fe_2Ti_3O_{18}$, $Tb_{0.90}Bi_{5.1}Fe_2Ti_3O_{18}$ with $Bi_6Ti_3Fe_2O_{18}$ thin films. The out-of-plane polarization response is weak for layered Aurivillius materials, but can be locally probed by boosting the signal by scanning at the tip/sample contact resonance frequency (300–310 kHz) in the DART-VPFM mode, which is a scanning mode designed to avoid the effects of topographical cross-talk or artefacts.[44,45] The difference between these two types of pointed opposite domains is 180°. Generation of macroscopic ferroelectric hysteresis involves nucleation and domain growth as a result of the accumulation of multi-domains while in the case of PFM, local hysteresis involves growth and nucleation of a usually a single domain below the tip-sample contact area at the submicron scale. Here, we have extracted the out-of-plane polarization loops and locally associated in-plane polarization with out-of-plane domains of $Bi_6Ti_3Fe_2O_{18}$, $Tb_{0.40}Bi_{5.6}Fe_2Ti_3O_{18}$, and $Tb_{0.90}Bi_{5.1}Fe_2Ti_3O_{18}$ thin films at room temperature via lateral switching spectroscopy (at 20 kHz below the tip/sample resonance frequency) and vertical switching spectroscopy (DART-SSPFM generated at a tip/sample resonance frequency of 300–310 kHz) using a triangular step waveform cycled twice at 0.2 Hz (comprised V_{dc} in steps on and off) and with an AC signal of 5.5 V [Figs. 3(a)–3(f)]. It should be noted that the associated in-plane polarization response is extracted from the domain oriented along out-of-plane showing that it exhibits some component along the in-plane (in general, in Aurivillius phase materials, the in-plane piezoresponse from out-of-plane domains is attributed due to the Aurivillius phase grain tilt along the out-of-plane)). These loops were generated at 10 different points (positions) on each of the two selected 0° (c) (encircled red) and 180° (c+) (encircled green) oriented domains [Figs. 3(a)–3(f)]. The room temperature local out-of-plane piezoelectric loops [Fig. 3(e)] demonstrate that the Tb substitution enhances ferroelectric polarization systematically, since we observe out-of-plane remnant piezoelectric and saturation piezoelectric values which are higher for $Tb_{0.40}Bi_{5.6}Fe_2Ti_3O_{18}$ and (±17 pm/V and ±20 pm/V) and $Tb_{0.90}Bi_{5.1}Fe_2Ti_3O_{18}$ (±31 pm/V and ±35 pm/V) compared with $Bi_6Ti_3Fe_2O_{18}$ (±6.19 pm/V and ±7.55 pm/V) thin films. The in-plane and out-of-plane

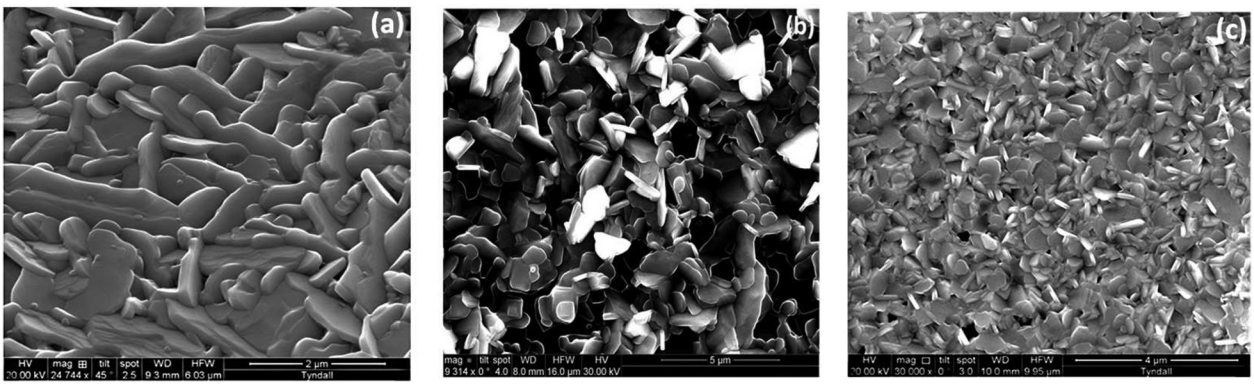

FIG. 2. Representative SEM images (a)–(c) for $Bi_6Fe_2Ti_3O_{18}$, $Tb_{0.40}Bi_{5.6}Fe_2Ti_3O_{18}$, and $Tb_{0.9}Bi_{5.1}Fe_2Ti_6O_{18}$ thin films, respectively, deposited on the sapphire substrate.

polarization response of $Bi_6Ti_3Fe_2O_{18}$, $Tb_{0.40}Bi_{5.6}Fe_2Ti_3O_{18}$, and $Tb_{0.90}Bi_{5.1}Fe_2Ti_3O_{18}$ thin films was investigated by using single-frequency piezoresponse force microscopy (SPFM) at frequency below the tip/sample contact resonance frequency (we usually use 20 kHz in the SPFM mode in order to avoid any possible topographical cross-talk, which usually affect piezoresponse). The in-plane and out-of-plane amplitude and phase response (SPFM at 20 kHz) from $Bi_6Ti_3Fe_2O_{18}$, $Tb_{0.40}Bi_{5.6}Fe_2Ti_3O_{18}$, and $Tb_{0.90}Bi_{5.1}Fe_2Ti_3O_{18}$ thin films [Figs. 4(a)–4(h)] at room temperature demonstrate that these films have dominant naturally self-polarized piezoelectric domains lying along the in-plane a-axis [Figs. 4(a) and 4(e)] with preferential orientation either along 0° or 180° [Figs. 4(c) and 4(g)]. Weak piezoelectric response was observed along the out-of-plane [Figs. 4(b), 4(d), 4(f), and 4(h)]. A comparison with out-of-plane images generated at the same area using the single-frequency modes demonstrates that the samples exhibit weaker out-of-plane *c*-axis response with respect to the PFM tip. The in-plane ferroelectric switching polarization reversal loops [Figs. 5(a) and 5(b)] (generated below the tip/sample contact frequency of 20 kHz using triangular step waveform cycled twice at 0.2 Hz on 10 different points on each of the two selected 0° (c^-) (encircled red) and 180° (c^+) (encircled green) oriented domains [Figs. 4(a)–4(e)] demonstrate that the piezoelectric response (amplitude response) increases with an increase in Tb substitution. In-plane piezoresponses are higher for $Tb_{0.40}Bi_{5.6}Fe_2Ti_3O_{18}$ (±92 pm/V and ±73 pm/V) and $Tb_{0.90}Bi_{5.1}Fe_2Ti_3O_{18}$ (±135 pm/V and ±102 pm/V), rather than $Bi_6Ti_3Fe_2O_{18}$, (±47 pm/V and 37 pm/V) thin films. Furthermore, these results confirm that the lateral in-plane a-axis saturation piezoresponse (±47 pm/V, 92 pm/V and ±135 pm/V at 20 kHz) observed for these films is higher than the vertical out-of-plane saturation piezoresponse (±9.3 pm/V, 20 pm/V, and ±37 pm/V at 300–310 kHz). No coupled vertical polarization reversal signatures (at a tip/sample contact frequency of 300 kHz) from the in-plane a-axis oriented domain were observed, clearly demonstrating the existence of major polarization only along the in-plane *a*-axis. The potential for $Bi_6Ti_3Fe_2O_{18}$, $Tb_{0.40}Bi_{5.6}Fe_2Ti_3O_{18}$, and $Tb_{0.90}Bi_{5.1}Fe_2Ti_3O_{18}$ thin films as lead free ferroelectric materials with the ability to retain piezoelectric properties at the elevated temperature (200 °C) was explored by generating local in-plane saturation loops as a function of temperature (room → 200 °C) as is illustrated in Fig. 5(b). These responses were collected and analysed by generating and averaging a number ($n = 10$) of saturation loops at 20 kHz on the selected (encircled red and green) domains as a function of temperature and rough average piezoresponse polarization values are extracted. It is observed that the $Tb_{0.40}Bi_{5.6}Fe_2Ti_3O_{18}$ and $Tb_{0.90}Bi_{5.1}Fe_2Ti_3O_{18}$ thin films have higher in-plane polarization saturation (±201 pm/V and ±154 pm/V) and remanence (±172 pm/V and ±125 pm/V), rather than $Bi_6Ti_3Fe_2O_{18}$ saturation polarization (±65 pm/V) and remanence (44 pm/V) at elevated temperature (up to 200 °C). The in-plane saturation polarization and remanence increase slightly (no significant) up to 100 °C, however, the response starts decrease after 100 °C [Fig. 5(b)]. This slight increase may be attributed to the removal of surface residues at higher temperatures such as evaporation or removal of water molecules from the film surface.[18] These results clearly demonstrate that $Bi_6Ti_3Fe_2O_{18}$, $Tb_{0.40}Bi_{5.6}Fe_2Ti_3O_{18}$, and $Tb_{0.90}Bi_{5.1}Fe_2Ti_3O_{18}$ thin films have potential and could be utilized in elevated temperature device applications.

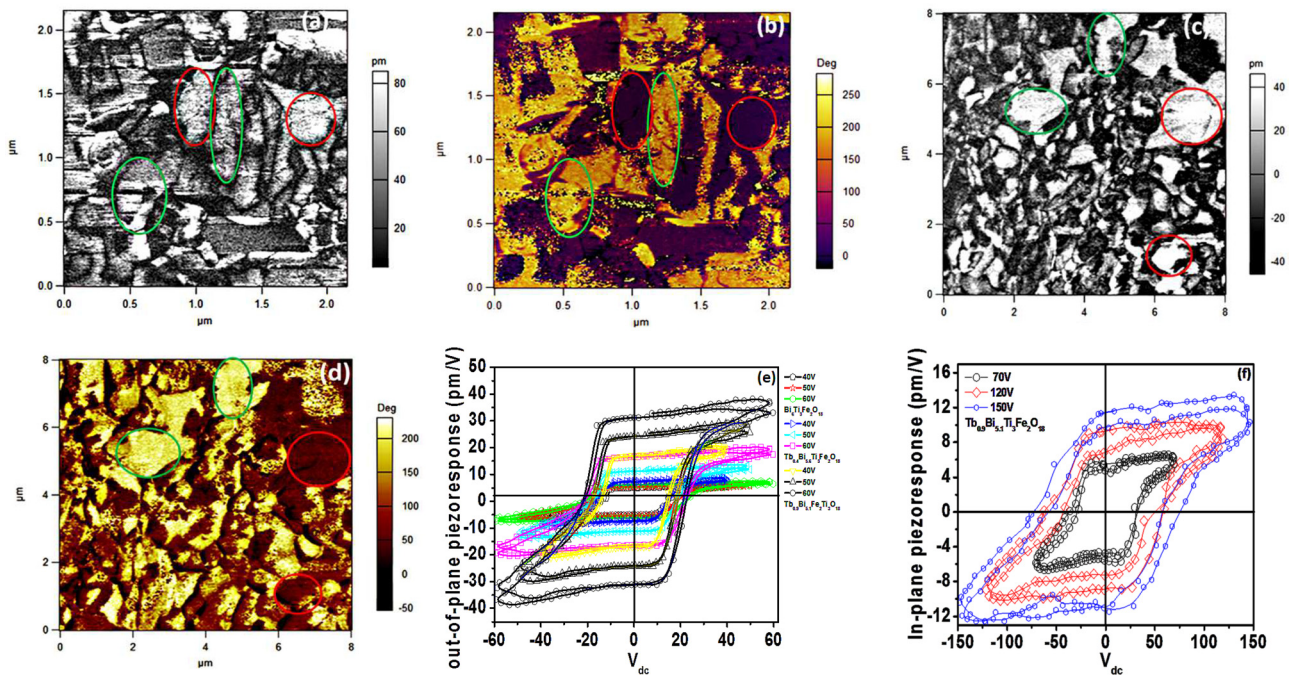

FIG. 3. Dual AC Resonance Tracking (DART) PFM amplified images of (a) amplitude response, (b) phase response of the $Tb_{0.40}Bi_{5.6}Fe_2Ti_3O_{18}$ thin film on the sapphire substrate: (c) amplitude response, (d) phase response of the $Tb_{0.9}Bi_{5.1}Fe_2Ti_6O_{18}$ thin film on the sapphire substrate, and (e) comparison of local out-of-plane piezoelectric loops for $Bi_6Fe_2Ti_3O_{18}$, $Tb_{0.40}Bi_{5.6}Fe_2Ti_3O_{18}$, and $Tb_{0.9}Bi_{5.1}Fe_2Ti_6O_{18}$ thin films generated via Vertical DART-PFM switching spectroscopy, and (f) in-plane lateral piezoelectric loops for $Tb_{0.9}Bi_{5.1}Fe_2Ti_6O_{18}$ domains extracted via single frequency switching PFM at 20 kHz after the removal of an applied DC bias.

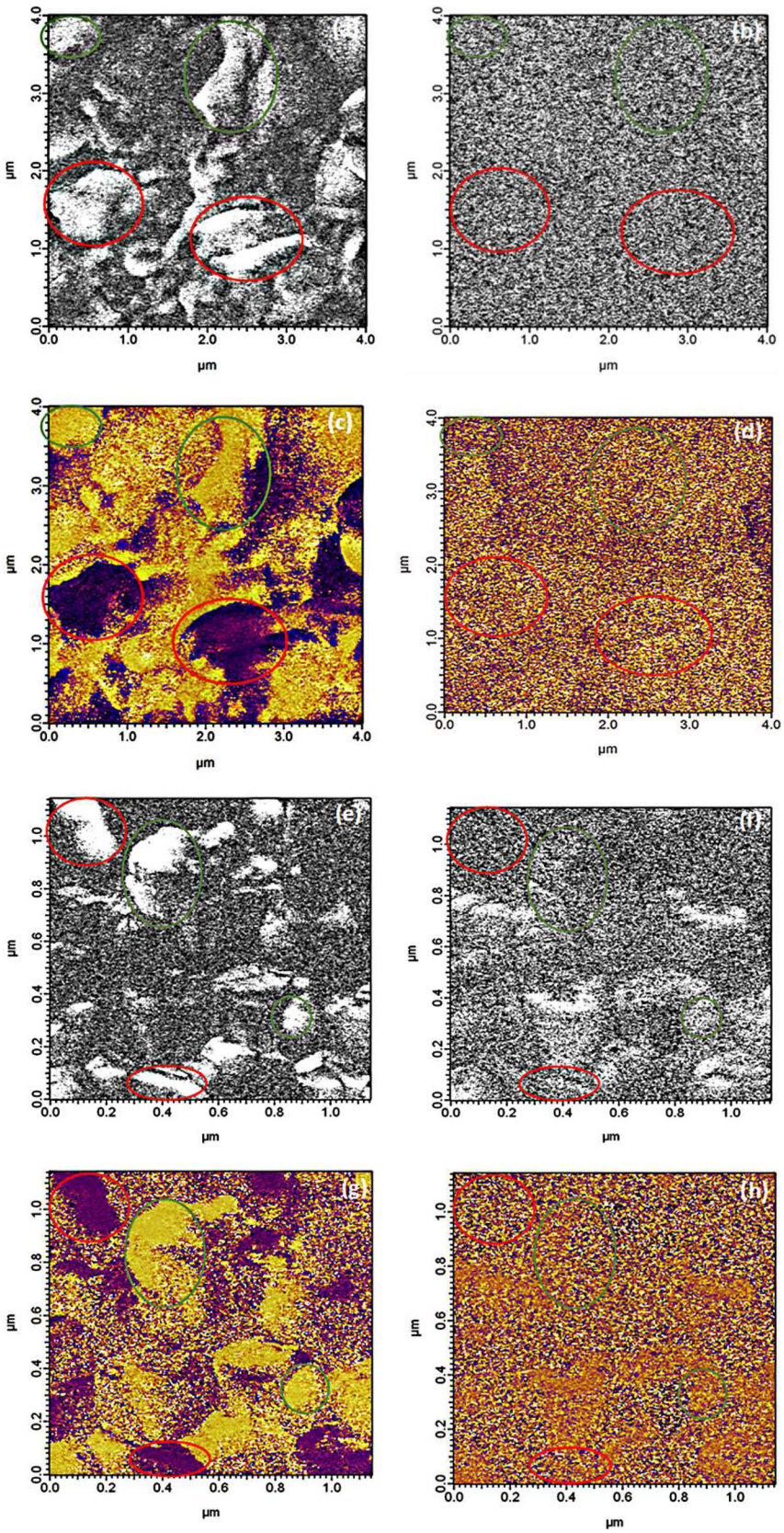

FIG. 4. Single frequency piezoresponse force microscopy (SPFM) (a) in-plane Amplitude, (b) out-of-plane PFM Amplitude response, (c) in-plane phase, (d) out-of-plane phase response for $Tb_{0.40}Bi_{5.6}Fe_2Ti_3O_{18}$ thin films, (e) in-plane Amplitude, (f) out-of-plane PFM Amplitude response, (g) in-plane phase, and (h) out-of-plane phase response for the $Tb_{0.9}Bi_{5.1}Ti_3Fe_2O_{18}$ thin film deposited on the sapphire substrate.

Conventional random access memory (RAM) is based on top/bottom electrodes as capacitive systems. Commonly used materials for RAM are lead-based (PZT) perovskites which exhibit relatively high ferroelectric polarization (20–70 $\mu C/cm^2$).[46,47] But these materials suffer from serious challenges when integrated in such technologies such as polarization fatigue temperature instability or evaporation of deleterious PbO, etc. These serious concerns could be overcome by using alternative lead-free materials such as the Aurivillius layered structure identified as potential

alternatives, given that they are lead free piezoelectric/ferroelectric materials exhibiting relatively high Curie temperatures (Tc generally in the range 230–675 °C),[48–50] with in-plane (*a*-axis) ferroelectric remnant (P_r) polarizations in the range of 5.4–29 $\mu C/cm^2$ (Refs. 51–53) and demonstrate fatigue-free switching and high temperature (200 °C) data read/write stabilities.[18,54] Aurivillius phase materials are not suitable for integration in RAM devices based on conventional top/bottom electrode systems because of their relatively weak out-of-plane ferroelectric polarizations. The macroscopic in-plane potential of $Bi_6Ti_3Fe_2O_{18}$, $Tb_{0.40}Bi_{5.6}Fe_2Ti_3O_{18}$, and $Tb_{0.90}Bi_{5.1}Fe_2Ti_3O_{18}$ (±130 nm) thin films was explored using in-plane interdigitated electrodes (IDEs) [Fig. 5(c)], possessing 32 fingers, 8 μm interfinger spacing, and finger widths of 2 μm, thickness of 100 nm using a frequency of 100 Hz. The schematic Fig. 5(d) illustrates that the direction of the applied electric field (E) across the IDE fingers is along the in-plane *a*-axis of these films. Hence, electric field (E) lines that interact with the in-plane *a*-axis of the Aurivillius films crystal result in in-plane saturation hysteresis loops. These measurements confirm that the materials in this study exhibit in-plane ferroelectric polarization (P_x) which increases with an increase in the applied in-plane electric field (E_3) up to the in-plane saturation field (P_{sx}), and charge conduction (Q) is suppressed above the minimum required in-plane coercive field (E_{3x}) of these films [Fig. 5(e)]. Ferroelectric parameters such as in-plane saturation (P_{sx}), remanence polarization (P_{rx}), and coercive field (E_{3c}) were extracted from the ferroelectric polarization loops [Fig. 5(e)]. P_{sx} and E_{3c} are extrinsic properties and depend on the spacing between IDEs, roughness, texture, and density of the film. The hysteresis loops

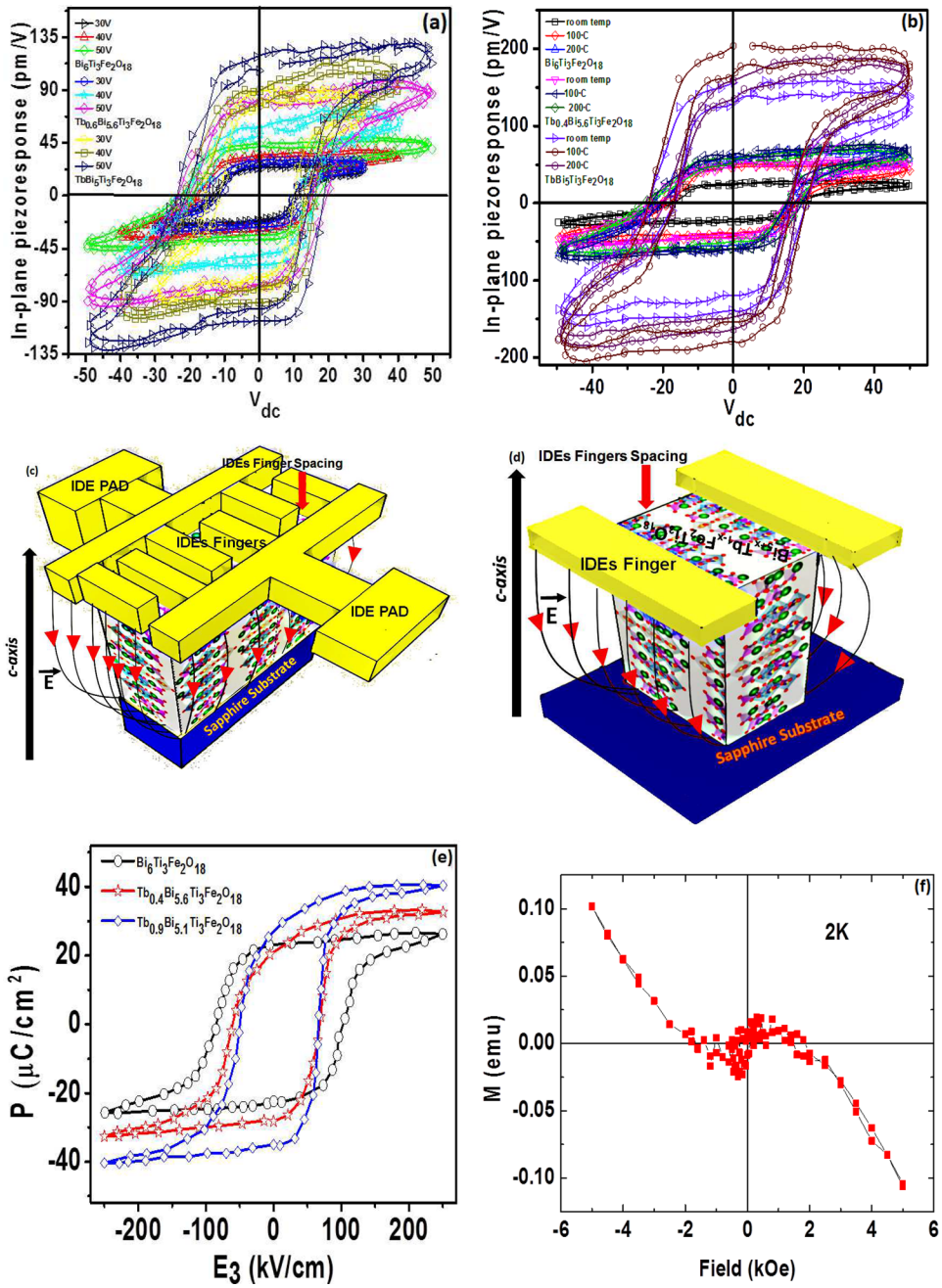

FIG. 5. (a) Single frequency in-plane PFM loops extracted using single frequency at 20 kHz after the removal of an applied DC bias, (b) comparison between the temperature dependent in-plane PFM ferroelectric polarizations loops generated at 20 kHz via single frequency switching spectroscopy; schematic (c) represents the IDE test structure on the crystal structure of the $m = 5$ Aurivillius phase $Tb_{1-x}Bi_{5+x}Fe_2Ti_3O_{18}$ along the ⟨110⟩ direction with five perovskite units sandwiched between two bismuth oxide block thin films deposited on a sapphire substrate (d) illustrating the effect of the in-plane electric field of lines on an in-plane a-axis polarization plane associated within the IDEs (e) in-plane ferroelectric polarization hysteresis using interdigitated electrodes (IDEs) generated from $Bi_6Ti_3Fe_2O_{18}$, $Tb_{0.40}Bi_{5.6}Fe_2Ti_3O_{18}$, and $Tb_{0.9}Bi_{5.1}Ti_3Fe_2O_{18}$ thin films; (f) magnetic response from the $Tb_{0.9}Bi_{5.1}Ti_3Fe_2O_{18}$ thin film magnetic hysteresis loop at 2 K.

generated in a driven electric field (E_3) $\pm 245\,kV/cm^2$ confirm the required saturation field as illustrated in Fig. 5(e). The in-plane saturation (P_{sx}) and remanence (P_{rx}) polarization for $Bi_6Ti_3Fe_2O_{18}$ are $\pm 26.16\,\mu C/cm^2$ and $\pm 22\,\mu C/cm^2$, whereas, $\pm 32.75\,\mu C/cm^2$ and $\pm 22.11\,\mu C/cm^2$, $\pm 40.30\,\mu C/cm^2$ and $\pm 28.5\,\mu C/cm^2$ for $Tb_{0.40}Bi_{5.6}Fe_2Ti_3O_{18}$ and (± 130 nm) thin films, respectively. It is clearly observed that in-plane saturation (P_{sx}) and remanence polarization (P_{rx}) are correlated with Tb substitution and increase with the increase in Tb substitution. The in-plane macroscopic switching polarization observed for $Tb_{0.40}Bi_{5.6}Fe_2Ti_3O_{18}$ and $Tb_{0.9}Bi_{5.1}Fe_2Ti_3O_{18}$ thin films are comparable with values of remnant (P_r) polarization values of PZT $[Pb(Zr_{0.52}Ti_{0.48})]O_3$, $P_r = 12$–$65\,\mu C/cm^2$,[55,56] $SrBi_4Ti_4O_{15}$ ($P_r = \pm 5$–$29\,\mu C/cm^2$),[57–59] and $SrBi_2Ta_2O_9$ (SBT) ($P_r = \pm 7.5$–$12\,\mu C/cm^2$)[52,60] based systems common materials in FeRAMs with conventional top/bottom electrodes.[61] No ferromagnetic signature were observed for $Bi_6Ti_3Fe_2O_{18}$ and $Tb_{0.40}Bi_{5.6}Fe_2Ti_3O_{18}$ thin films. However, a weak ferromagnetic signature was observed for the $Tb_{0.9}Bi_{5.1}Fe_2Ti_3O_{18}$ sample. These magnetic loops were generated using SQUID (superconducting quantum interference device) magnetization measurements as a function of magnetic field at temperatures of 2 K as are shown in Fig. 5(f). It should be noted that due to high noise level extraction of magnetic parameters such as M_r, M_s, and H_c from observed weak signature ferromagnetic signatures is quite difficult. Due to the plate-like nature of Aurivillius phase grains, the thickness (100 ± 30 nm) varies across the sample. We have calculated the average $Tb_{0.9}Bi_{5.1}Fe_2Ti_3O_{18}$ thin film thickness by taking ~50 cross-section thickness measurements across the sample piece via HR-SEM. In addition, the porosity was taken into account as a 2.70% area of the substrate was not covered with the $Tb_{0.9}Bi_{5.1}Fe_2Ti_3O_{18}$ thin film. It is observed from Fig. 5(f), which, at positive (negative) high field, the downward (upward) direction of the curve originates from the diamagnetic substrate.

HRTEM [Jeol (21)00, 200 kV; double tilt sample holder] [Figs. 6(a)–6(c)] demonstrates that $Tb_{0.40}Bi_{5.6}Fe_2Ti_3O_{18}$ thin films is $m = 5$ layers, however, exhibit few regions where the Aurivillius phase unit (c-lattice) parameter is in the range of 3.5–4.5 nm [Figs. 6(b) and 6(c)] suggesting that there are parts of the sample having intergrowths of different Aurivillius phases having 3–5 perovskite blocks per half unit cell. This is also confirmed from the XRD profile where the (119) reflection peak is observed from the secondary minor $m = 4$ layer $Bi_5Ti_3FeO_{15}$ impurity phase. However, the c-lattice for the $Tb_{0.9}Bi_{5.1}Fe_2Ti_3O_{18}$ thin films is 4.8 nm confirming it has 5 perovskite blocks per half unit cell. Both $Tb_{0.40}Bi_{5.6}Fe_2Ti_3O_{18}$ and $Tb_{0.9}Bi_{5.1}Fe_2Ti_3O_{18}$ thin films are inhomogeneous in terms of their coverage of the sapphire substrates and are very thin patchy films with an average thickness of ~100 nm. In order to investigate whether Tb was successfully incorporated into the Aurivillius phase structure in both the $Tb_{0.40}Bi_{5.6}Fe_2Ti_3O_{18}$ and $Tb_{0.9}Bi_{5.1}Fe_2Ti_3O_{18}$ thin film samples and to investigate whether the observed ferromagnetism in the $Tb_{0.9}Bi_{5.1}Fe_2Ti_3O_{18}$ sample can be reliably assigned to the Aurivillius phase and not due to the presence

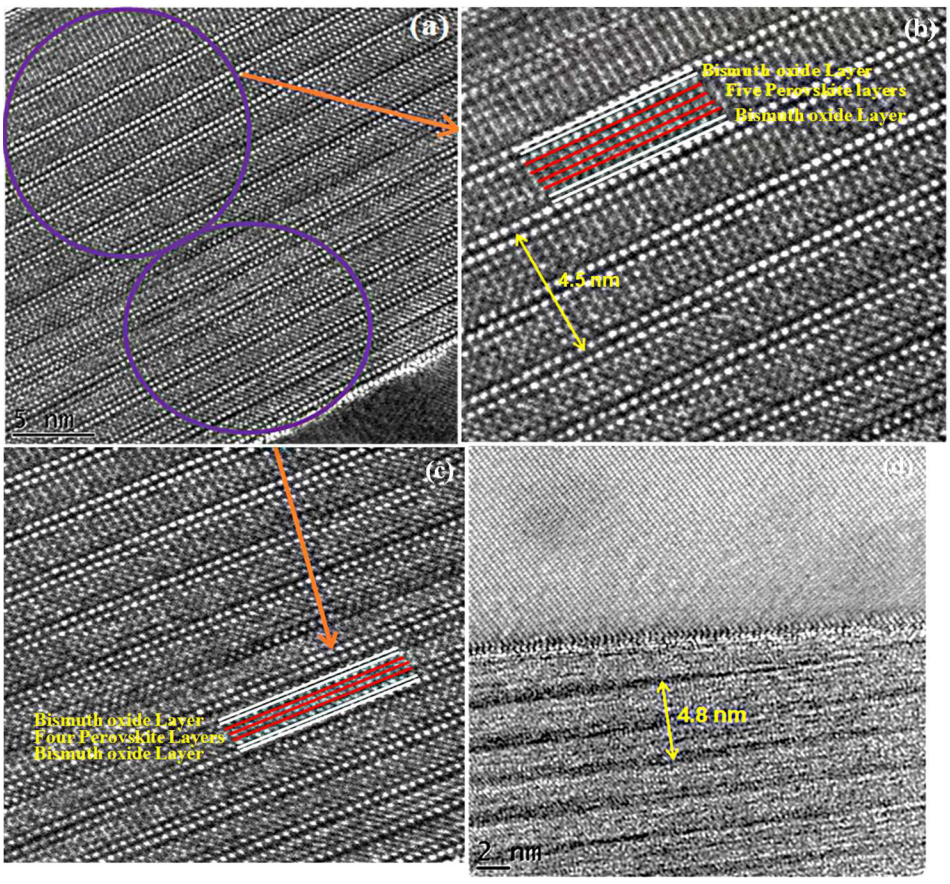

FIG. 6. Microstructural analysis – (a) HRTEM cross-section image for $Tb_{0.40}Bi_{5.6}Fe_2Ti_3O_{18}$ thin films (b) regions in the $Tb_{0.40}Bi_{5.6}Fe_2Ti_3O_{18}$ thin film uniform m = 5 layered Aurivillius structure (c) highlighted m = 5 layers Tb $Tb_{0.40}Bi_{5.6}Fe_2Ti_3O_{18}$ have some regions with m = 4 layer structures (d) HRTEM cross-section image for $Tb_{0.9}Bi_{5.1}Ti_3Fe_2O_{18}$ thin films.

of trace levels of magnetic impurities, further compositional, morphological, and structural analysis was performed.

HR-SEM-EDX surface scans were performed over short (2 h) and long (72 h) time periods on relatively large sample areas of the $Tb_{0.40}Bi_{5.6}Fe_2Ti_3O_{18}$ (2250 μm^2) and $Tb_{0.9}Bi_{5.1}Fe_2Ti_3O_{18}$ (1600 μm^2) thin films and the morphology, composition, and volume of any second-phase magnetic and ferroelectric inclusions were assessed. No Tb/Fe rich secondary phases were detected over sample areas of $42 \times 38\ \mu m^2$ during 2 h scans for $Tb_{0.40}Bi_{5.6}Fe_2Ti_3O_{18}$, indicating that if impurities are present, they are there at relatively low levels. Hence, we have performed longer time periods, 72 h, EDX scan to increase the signal-to-noise ratio elemental mapping scan across 2244 μm^2 of the sample surface for the $Tb_{0.40}Bi_{5.6}Fe_2Ti_3O_{18}$ thin films (as illustrated in Fig. 7). The subtraction of BiLα EDX from TbKα and FeKα signals demonstrates no prominent variations later from the average value [Figs. 7(a)–7(d)]. FeKα minus BiLα map [Fig. 7(d)] TbKα minus BiLα map [Fig. 7(c)], revealed that Tb is uniformly distributed over the whole film. No Tb rich impurities were observed in $Tb_{0.40}Bi_{5.6}Fe_2Ti_3O_{18}$ thin films. However, these elemental mapping revealed that there are few Fe rich areas in the diameter range of 500 nm [as encircled in Fig. 7(d)]. The net iron rich impurities present in $Tb_{0.40}Bi_{5.6}Fe_2Ti_3O_{18}$ thin films at a volume fraction of 0.026%. These mappings for $Tb_{0.40}Bi_{5.6}Fe_2Ti_3O_{18}$ analysis reveal that Tb seems to be patchily present in the main phase with varied ratios of Bi: Tb of 15: 1. Since we have previously noted the elemental variations for over the CSD and LICVD grown $Bi_6Ti_{2.99}Fe_{1.46}Mn_{0.55}O_{18}$ system,[14,15] hence, in order to confirm the substitution of Tb to form $Tb_{0.40}Bi_{5.6}Fe_2Ti_3O_{18}$ thin films, we performed elemental analysis on individual Aurivillius phase grains. We selected 15 grains from a lamella of the $Tb_{0.40}Bi_{5.6}Fe_2Ti_3O_{18}$ thin films followed by normalization of Bi: Tb: Fe: Ti ratios, shows average ratio Bi (5.6): Tb (0.4): Fe (2): Ti (3) and composition $Tb_{0.40}Bi_{5.6}Fe_2Ti_3O_{18}$. Hence, it is confirmed that 0.40 mol. % of Tb is successfully substituted in $Tb_{0.40}Bi_{5.6}Fe_2Ti_3O_{18}$ thin films. However, no ferromagnetic signatures were observed for these films. Similarly, a 72 h HR-SEM-EDX scan was conducted over the area 1600 μm^2 on $Tb_{0.9}Bi_{5.1}Fe_2Ti_3O_{18}$ thin films. The subtraction of BiLα EDX from TbKα and FeKα signals demonstrates the subtle variations in the later from the average value [Figs. 7(e)–7(h)]. The resulting compositions are shown in Fig. 7(f) FeKα minus BiLα map Fig. 7(h) TbKα minus BiLα map, revealed some bright regions with higher Tb and Fe contents (4% volume fraction to the parent $Tb_{0.9}Bi_{5.1}Fe_2Ti_3O_{18}$ phase). These subtractions of spectral lines are made on the assumptions that the average compositional contents of Tb and Fe remain constant over the whole film. The small changes from the constant contents are monitored in these scans. The cross-section EDX across the Tb/Fe

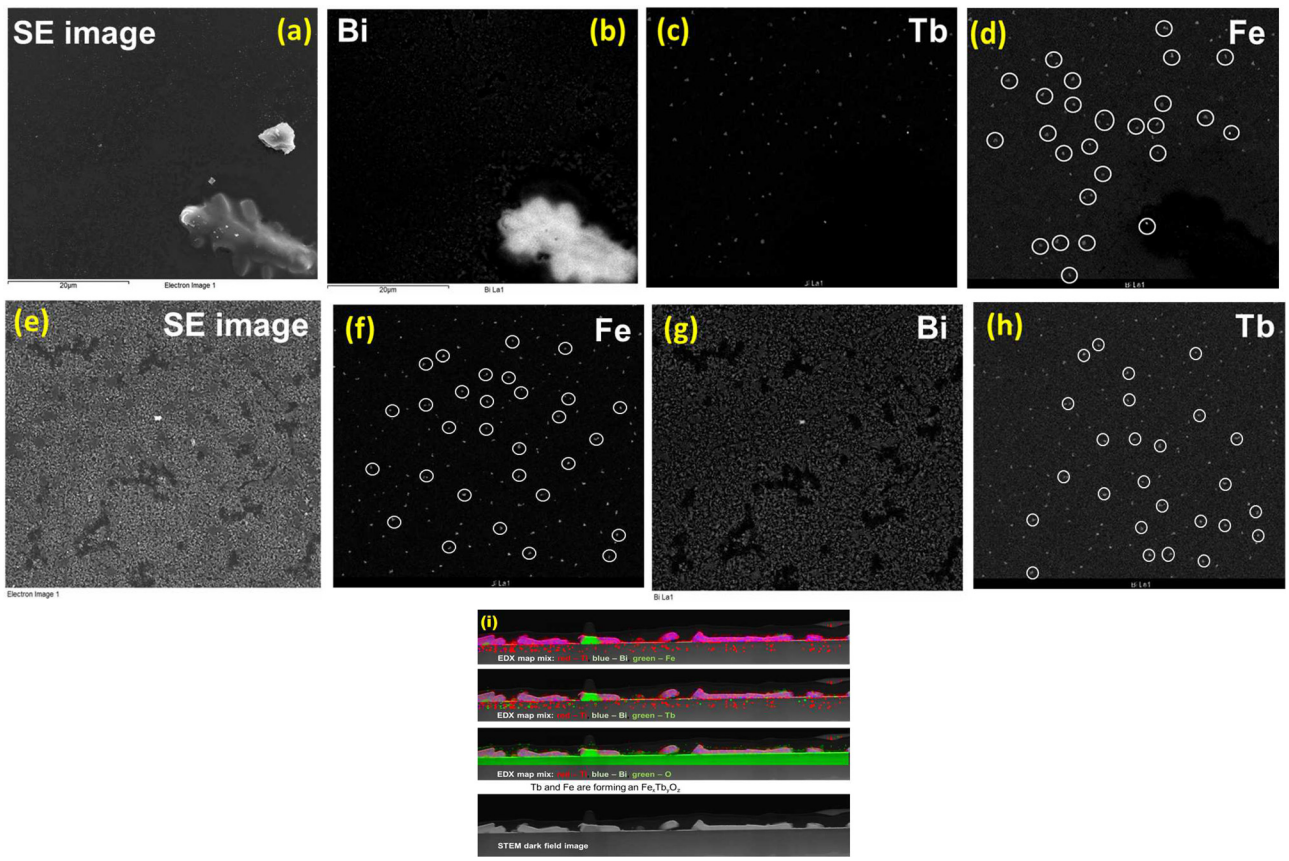

FIG. 7. Compositional analysis: representative cross-sectional EDX map of $Tb_{0.40}Bi_{5.6}Fe_2Ti_3O_{18}$ (2244 μm^2) thin films on *c*-plane sapphire (a) secondary electron image, (b) Bi distribution over the film, (c) Tb minus Bi distribution, (d) Fe minus Bi distribution from $Tb_{0.40}Bi_{5.6}Fe_2Ti_3O_{18}$ thin films; compositional analysis: representative cross-sectional EDX map of $Tb_{0.9}Bi_{5.1}Ti_3Fe_2O_{18}$ (1600 μm^2) thin films on *c*-planer sapphire, (e) secondary electron image, (g) Bi distribution over the film, (f) Fe minus Bi distribution, (h) Tb minus Bi distribution from $Tb_{0.9}Bi_{5.1}Ti_3Fe_2O_{18}$ thin films, and (i) HRTEM-EDX localized elemental mapping from $Tb_{0.9}Bi_{5.1}Ti_3Fe_2O_{18}$ thin films showing cubic magnetic inclusion of the $Fe_xTb_yO_z$ (x∼y)-type phase.

inclusions confirms that the $Tb_{0.9}Bi_{5.1}Fe_2Ti_3O_{18}$ thin films have potential ferromagnetic oxide inclusion of $Fe_xTb_yO_z$. In order to investigate the structure and possible composition of the inclusions to investigate whether they could have an effect on the magnetic response, site specific localized elemental mapping was performed [Fig. 7(i)] across a section of the sample via STEM with EDX. It can be seen from EDX elemental mapping that there is clear evidence of Fe/Tb/Bi rich inclusions. These inclusions also contained inhomogeneous Ti. All these elemental maps were colour coded (red – Ti, green – Tb/Fe/O, blue – Bi), added up into a red-green-blue (RGB) image and superimposed onto the SEM image, all done within the Oxford INCA software. From these localized mapping, we observe clear evidence of some areas with clusters of $Fe_xTb_yO_z$. The inclusions shown in Fig. 7(e) are homogenously spread (72 h EDX maps across 1600 μm^2 revealed approximately 80 Fe/Tb rich inclusions in with grain sizes having diameters in the range of 100–500 nm) throughout the sample cross-section. It has been reported that rare earth elements such as $TbMnO_3$[62] hold large magnetic moments, outstanding magnetocrystalline anisotropy, magnetostriction, and large ionic radii. The substitution of rare earth Tb as $Fe_xTb_yO_z$ may cause structural distortion and magnetic coercivity.[63] Furthermore, ferrimagnetic responses have been reported for the cubic spinel Fe_3O_4 (M_s = 70–80 emu/g),[64] however, in complex $Co_{1-x}Tb_xFe_2O_4$ spinel systems, the magnetic saturation (M_s) values decrease with increased Tb substitution and found in the range (Ms = 63–67 emu/g).[65] The results from literature and data analysed suggest that Tb substituted $Tb_{0.9}Bi_{5.1}Fe_2Ti_3O_{18}$ thin films are not likely to be single-phase multiferroic materials, since, due to the presence of secondary magnetic $Fe_xTb_yO_z$ impurity at a volume fraction of 4%, this accounts for the measured weak magnetic signature.

IV. CONCLUSIONS

Here, in this work, we investigate Tb substitution at the A-site of m = 5 layered Aurivillius phase $Bi_6Ti_3Fe_2O_{18}$ thin films deposited on 2″ C-M plane (0001) oriented sapphire substrates synthesized by a chemical solution deposition (CSD) process. The effect of Tb substitution on multifunctional physical properties such as piezoelectricity, ferroelectricity, and ferromagnetism was probed. Single-frequency and DART piezoresponse force microscopy (PFM) confirm that $Bi_6Ti_3Fe_2O_{18}$, $Tb_{0.40}Bi_{5.6}Fe_2Ti_3O_{18}$, and $Tb_{0.90}Bi_{5.1}Fe_2Ti_3O_{18}$ thin films are piezoelectric and exhibit higher piezoelectric responses along the in-plane a-axis compared with the out-of- plane direction. The analysis reveals that Tb substituted $Tb_{0.40}Bi_{5.6}Fe_2Ti_3O_{18}$ and $Tb_{0.90}Bi_{5.1}Fe_2Ti_3O_{18}$ thin films exhibit higher in-plane (piezoresponses at saturation = ±201 pm/V and ±154 pm/V) and remnant piezoresponses = ±172 pm/V and ±125 pm/V at 20 kHz) and out-of-plane (piezoresponses at saturation = ±20 pm/V and ±35 pm/V) and remnant piezoresponses = ±17 pm/V and ±31 pm/V) at 20 kHz), polarization compared with the in-plane and out-plane polarization from $Bi_6Ti_3Fe_2O_{18}$ (piezoresponse at saturation = ±65 pm/V and remnant piezoresponses =44 pm/V) and piezoresponse at saturation = ±7.55 pm/V and remnant piezoresponse = ±6.19 pm/V) thin films. In-significant changes in local in-plane and out-of-plane piezoresponse with increases in temperature (200 °C) demonstrates polarization stability at elevated temperature. Macroscopic in-plane ferroelectric switching polarization loops investigated by depositing in-plane interdigitated electrodes (IDEs) on $Bi_6Ti_3Fe_2O_{18}$, $Tb_{0.40}Bi_{5.6}Fe_2Ti_3O_{18}$, and $Tb_{0.90}Bi_{5.1}Fe_2Ti_3O_{18}$ thin films, confirm that these films exhibit saturation (P_s) and remanence (P_r) polarization values of ±32.75 $\mu C/cm^2$ and ±22.11 $\mu C/cm^2$, ±40.30 $\mu C/cm^2$ and ±28.5 $\mu C/cm^2$, and ±26.16 $\mu C/cm^2$ and ±22 $\mu C/cm^2$. These values are comparable with the values of commonly used FeRAM based materials such as $SrBi_2Ta_2O_9$ (SBT),[66,67] $SrBi_4Ti_4O_{15}$ (SBT),[68] and $SrBi_2(Ta_{0.5}Nb_{0.5})_2O_9$ (SBNT),[69] indicating that $Bi_6Ti_3Fe_2O_{18}$, $Tb_{0.40}Bi_{5.6}Fe_2Ti_3O_{18}$, and $Tb_{0.90}Bi_{5.1}Fe_2Ti_3O_{18}$ are suitable for in-plane Fe-RAMs.[61] Furthermore, the increase in ferroelectric polarization (P_x) with Tb substitution $Tb_{0.40}Bi_{5.6}Fe_2Ti_3O_{18}$, $Tb_{0.9}Bi_{5.1}Fe_2Ti_3O_{18}$ as compared with $Bi_6Ti_3Fe_2O_{18}$ thin films confirms that Tb substitution affects and influences the ferroelectric properties (it should be noted that Tb is successfully substituted and forms $Tb_{0.40}Bi_{5.6}Fe_2Ti_3O_{18}$ while $Tb_{0.9}Bi_{5.1}Fe_2Ti_3O_{18}$ have no conclusive evidence Tb substitution). STEM-EDX imaging confirm that these films are of the $m = 5$ Aurivillius phase with no ferroelectric impurity phases such as effecting the ferroelectric properties. No ferromagnetic signatures were observed for $Bi_6Ti_3Fe_2O_{18}$ and $Tb_{0.40}Bi_{5.6}Fe_2Ti_3O_{18}$ thin film systems, however, a weak magnetic response was observed for $Tb_{0.9}Bi_{5.1}Fe_2Ti_3O_{18}$ thin films. STEM-EDX imaging for $Tb_{0.9}Bi_{5.1}Fe_2Ti_3O_{18}$ thin films identified magnetic inclusions of a $Fe_xTb_yO_z$ (x∼y)-type phase, present at a volume fraction of 4%. This data however implies that $Tb_{0.9}Bi_{5.1}Fe_2Ti_3O_{18}$ thin films are not likely to be ferromagnetic or multiferroic at room temperature, as the presence of secondary magnetic oxide phase $Fe_xTb_yO_z$ (x∼y) impurities account for the measured magnetic response in these films. It is important to note that this kind of discussion of possible magnetic impurity phase levels, and their effects, is often absent in previous studies reported on these novel types of materials. However, our group performed deep and thorough studies such as these to reach to conclusive results.

ACKNOWLEDGMENTS

The support of NANOMOTION Grant Agreement No. 290158, the 7th Framework Programme Marie Curie Initial Training Network, the Science Foundation Ireland (SFI) under the FORME Strategic Research Cluster Award No. 07/SRC/I1172, the Irish Higher Education Authority (HEA) PRTLI 3, and the HEA PRTLI4 Project INSPIRE is gratefully acknowledged. This publication has emanated from research conducted with the financial support of the Royal Society and Science Foundation Ireland University Research Fellowship UF 140263.

[1]P. Borisov and W. Kleemann, "Exchange bias and ferromagnetic coercivity in heterostructures with antiferromagnetic Cr_2O_3," J. Appl. Phys. **110**(3), 033917 (2011).

[2]J. M. Hu, Z. Li, J. Wang, and C. W. Nana, "Electric-field control of strain mediated magnetoelectric random access memory," J. Appl. Phys. **107**, 093912 (2010).

[3]N. Tiercelin, V. Preobrazhensky, P. Pernod, and A. Ostaschenko, "Enhanced magnetoelectric effect in nanostructured magnetostrictive thin film resonant actuator with field induced spin reorientation transition," Appl. Phys. Lett. **92**(6), 062904 (2008).

[4]L. E. Fuentes-Cobas, J. A. Matutes-Aquino, M. E. Botello-Zubiate, A. González Vázquez, M. E. Fuentes-Montero, and D. Chateigner, *Handbook of Magnetic Materials* (Elsevier, 2015), Vol. 24, pp. 237–322.

[5]N. Deepak, P. F. Zhang, L. Keeney, M. E. Pemble, and R. W. Whatmore, "Atomic vapor deposition of bismuth titanate thin films," J. Appl. Phys. **113**, 187207 (2013).

[6]B. Aurivillius, "Mixed bismuth oxides with layer lattices: I. Structure type of $CaBi_2B_2O_9$," Ark. Kemi **1**, 463–480 (1949).

[7]B. Aurivillius, "Mixed bismuth oxides with layer lattices II. Structure of $Bi_4Ti_3O_{12}$," Ark. Kemi **1**, 499–512 (1949).

[8]B. Aurivillius, "Mixed oxides with layer lattices. III. Structure of $BaBi_4Ti_4O_{15}$," Ark. Kemi **2**, 519–527 (1950).

[9]A. Faraz, N. Deepak, M. Schmidt, M. E. Pemble, and L. Keeney, "A study of the temperature dependence of the local ferroelectric properties of c-axis oriented $Bi_6Ti_3Fe_2O_{18}$ Aurivillius phase thin films: Illustrating the potential of a novel lead-free perovskite material for high density memory applications," AIP Adv. **5**, 087123 (2015).

[10]N. A. Hill, "First principles search for multiferroism in $BiCrO_3$," J. Phys. Chem. B **104**(29), 6694–6709 (2000).

[11]Y. H. Chu, L. W. Martin, M. B. Holcomb, M. Gajek, S. J. Han, Q. He, N. Balke, C. H. Yang, D. Lee, W. Hu, Q. Zhan, P. L. Yang, A. F. Rodriguez, A. Scholl, S. X. Wang, and R. Ramesh, "Electric-field control of local ferromagnetism using a magnetoelectric multiferroic," Nat. Mater. **7**(6), 478–482 (2008).

[12]T. Atou, H. Chiba, K. Ohoyama, Y. Yamaguchi, and Y. Syono, "Structure determination of ferromagnetic perovskite $BiMnO_3$," J. Solid State Chem. **145**, 639–642 (1999).

[13]A. M. Mulders, "Multiferroics: Magnetic moments under stress," Nat. Phys. **9**(7), 398–399 (2013).

[14]L. Keeney, T. Maity, M. Schmidt, A. Amann, N. Deepak, N. Petkov, S. Roy, M. E. Pemble, and R. W. Whatmore, "Magnetic field-induced ferroelectric switching in multiferroic Aurivillius phase thin films at room temperature," J. Am. Ceram. Soc. **96**(8), 2339–2357 (2013).

[15]A. Faraz, T. Maity, M. Schmidt, N. Deepak, S. Roy, M. E. Pemble, R. Whatmore, and L. Keeney, "Direct visualization of magnetic-field-induced magnetoelectric switching in multiferroic Aurivillius phase thin films," J. Am. Ceram. Soc. **100**, 975–987 (2017).

[16]M. Bibes and A. Barthélémy, "Multiferroics: Towards a magnetoelectric memory," Nat. Mater. **7**, 425–426 (2008).

[17]L. Keeney, S. Kulkarni, N. Deepak, M. Schmidt, N. Petkov, P. F. Zhang, and S. Cavill, "Room temperature ferroelectric and magnetic investigations and detailed phase analysis of Aurivillius phase $Bi_5Ti_3Fe_{0.7}Co_{0.3}O_{15}$ thin films," J. Appl. Phys. **112**(5), 052010 (2012).

[18]P. F. Zhang, N. Deepak, L. Keeney, M. E. Pemble, and R. W. Whatmore, "The structural and piezoresponse properties of c-axis-oriented Aurivillius phase $Bi_5Ti_3FeO_{15}$ thin films deposited by atomic vapor deposition," Appl. Phys. Lett. **101**(11), 112903 (2012).

[19]R. E. Jones, P. Zurcher, P. Chu, D. J. Taylor, Y. T. Lii, B. Jiang, P. D. Maniar, and S. J. Gillespie, "Memory applications based on ferroelectric and high-permittivity dielectric thin films," Microelectron. Eng. **29**(1–4), 3–10 (1995).

[20]R. E. Newnham, R. W. Wolfe, and J. F. Dorrian, "Structural basis of ferroelectricity in the bismuth titanate family," Mater. Res. Bull. **6**, 1029–1039 (1971).

[21]M. A. Zurbuchen, J. Lettieri, S. J. Fulk, Y. Jia, A. H. Carim, D. G. Schlom, and S. K. Streiffer, "Bismuth volatility effects on the perfection of $SrBi_2Nb_2O_9$ and $SrBi_2Ta_2O_9$ films," Appl. Phys. Lett. **82**, 4711–4713 (2003).

[22]X. Z. Zuo, M. L. Zhang, E. J. He, J. Yang, X. B. Zhu, and J. M. Dai, "Multiferroic property, dielectric response and scaling behaviour in Aurivillius $Bi_{4.25}Gd_{0.75}Fe_{0.5}Co_{0.5}Ti_3O_{15}$ ceramic," J. Alloys Compd. **695**, 2556–2562 (2017).

[23]X. Y. Mao, W. Wang, and X. B. Chen, "Electrical and magnetic properties of $Bi_5FeTi_3O_{15}$ compound prepared by inserting $BiFeO_3$ into $Bi_4Ti_3O_{12}$," Solid State Commun. **147**, 186–189 (2008).

[24]F. J. Yang, P. Su, C. Wei, X. Q. Chen, C. P. Yang, and W. Q. Cao, "Large magnetic response in $(Bi_4Nd)Ti_3(Fe_{0.5}Co_{0.5})O_{15}$ ceramic at room-temperature," J. Appl. Phys. **110**, 126102 (2011).

[25]A. Srinivas, M. M. Kumar, S. V. Suryanarayana, and T. Bhimasankaram, "Magnetoelectric measurements on $Bi_5Ti_3FeO_{15}$ and $Bi_6Ti_3Fe_2O_{18}$," Mater. Res. Bull. **34**(6), 989–996 (1999).

[26]V. Koval, I. Skorvanek, M. Reece, L. Mitoseriu, and H. Yan, "Effect of dysprosium substitution on crystal structure and physical properties of multiferroic $BiFeO_3$ ceramics," J. Eur. Ceram. Soc. **34**, 641 (2014).

[27]F. Xue, Q. Fu, D. Zhou, L. Zhou, Y. Hu, Z. Zheng, G. Jian, and L. Hao, "Structural evolution and physical properties of multiferroic $Bi_{0.9-x}La_{0.1}Pb_xFeO_{3-x/2}$ ceramics," J. Phys. D: Appl. Phys. **48**, 305004 (2015).

[28]A. Z. Simões, M. A. Ramírez, C. S. Riccardi, E. Longo, and J. A. Varela, "Ferroelectric properties and leakage current characteristics of $Bi_{3.25}La_{0.75}Ti_3O_{12}$ thin films prepared by the polymeric precursor method," J. Appl. Phys. **98**, 114103 (2005).

[29]P. Fang, H. Fan, J. Li, and F. Liang, "Lanthanum induced larger polarization and dielectric relaxation in Aurivillius phase $SrBi_{2-x}La_xNb_2O_9$ ferroelectric ceramics," J. Appl. Phys. **107**, 064104 (2010).

[30]C. M. Raghavan, J. W. Kim, J. Y. Choi, and S. S. Kim, "Effects of excessive Bi on structure and properties of Aurivillius $Bi_{5.25}La_{0.75}Fe_2Ti_3O_{18}$ thin films," New Phys. Sae Mulli. **65**(4), 311–316 (2015).

[31]C. L. Diao, H. W. Zheng, Y. G. Zhang, Z. Chen, and L. Fang, "Structure, photoluminescence and electrical properties of $BaBi_{3.5}Eu_{0.5}Ti_4O_{15}$ ceramics," Ceram. Int. **40**, 13827–13832 (2014).

[32]A. A. Alemi, R. Kashfi, and B. Shabani, "Preparation and characterization of novel Ln (Gd^{3+}, Ho^{3+} and Yb^{3+})-doped Bi_2MoO_6 with Aurivillius layered structures and photocatalytic activities under visible light irradiation," J. Mol. Catal. A: Chem. **392**, 290–298 (2014).

[33]V. A. Khomchenko, G. N. Kakazei, Y. G. Pogorelov, J. Araujo, M. V. Bushinsky, D. A. Kiselev, A. L. Kholkin, and J. A. Paixa, "Effect of Gd substitution on ferroelectric and magnetic properties of $Bi_4Ti_3O_{12}$," Mater. Lett. **64**, 1066–1068 (2010).

[34]T. Sarkar, S. A. Ivanov, E. A. Fortalnova, E. D. Politova, M. G. Safronenko, P. Nordblad, and R. Mathieu, "The role of Tb-doping on the structural and functional properties of $Bi_{4-x}Tb_xTi_3O_{12}$ ferroelectric phases with the Aurivillius type structure," Mater. Sci. Mater. Electron. **28**, 4914–4924 (2017).

[35]H. Singh and K. L. Yadav, "Dielectric, magnetic and magnetoelectric properties of La and Nb co doped bismuth ferrite," J. Phys.: Condens. Matter **23**, 385901 (2011).

[36]P. Ferrer, J. E. Iglesias, and A. Castro, "Synthesis of the Aurivillius Phase $SrBi_4Ti_4O_{15}$ by a Mechanochemical Activation Route," Chem. Mater. **16**(7), 1323–1329 (2004).

[37]R. Furushima, S. Tanaka, Z. Kato, and K. Uematsu, "Orientation distribution–Lotgering factor relationship in a polycrystalline material—as an example of bismuth titanate prepared by a magnetic field," J. Ceram. Soc. Jpn. **118**(10), 921–926 (2010).

[38]T. Siegrist, "Crystallographica - a software toolkit for crystallography," J. Appl. Crystallogr. **30**, 418–419 (1997).

[39]T. Maity, S. Goswami, D. Bhattacharya, and S. Roy, "Superspin glass mediated giant spontaneous exchange bias in a nanocomposite of $BiFeO_3$-$Bi_2Fe_4O_9$," Phys. Rev. Lett. **110**(10), 107201 (2013).

[40]M. Schmidt, A. Amann, L. Keeney, M. E. Pemble, J. D. Holmes, N. Petkov, and R. W. Whatmore, "Absence of evidence $\neq$ evidence of absence: Statistical analysis of inclusions in multiferroic thin films," Sci. Rep. **4**, 1–8 (2014).

[41]A. Lubk, S. Gemming, and N. A. Spaldin, "First-principles study of ferroelectric domain walls in multiferroic bismuth ferrite," Phys. Rev. B **80**, 104110–104118 (2009).

[42]S. Sankarrajan, K. Sakthipandia, and V. Rajendrana, "On-line phase transition in $La_{1-x}Sr_xMnO_3$ ($0.28 \leq x \leq 0.36$) perovskites through ultrasonic studies," Mater. Res. **15**(4), 517–521 (2012).

[43]C. R. Foschini, M. A. Ramirez, S. R. Simões, J. A. Varela, E. Longo, and A. Z. Simões, "Piezoresponse force microscopy characterization of rare-earth doped $BiFeO_3$ thin films grown by the soft chemical method," Ceram. Int. **39**(3), 2185–2195 (2013).

[44]B. J. Rodriguez, C. Callahan, S. V. Kalinin, and R. Proksch, "Dual-frequency resonance-tracking atomic force microscopy," Nanotechnology **18**(47), 475504–475506 (2007).

[45]S. V. Kalinin, Z. G. Ye, and A. L. Kholkin, "Piezoresponse force microscopy and nanoscale phenomena in polar materials," J. Appl. Phys. **112**(5), 051901 (2012).

[46]G. Rijnders and D. H. A. Blank, "Materials science: Build your own superlattice," Nature **433**, 369–370 (2005).

[47]D. Lee, S. M. Yang, T. H. Kim, B. C. Jeon, Y. S. Kim, J. G. Yoon, H. N. Lee, S. H. Baek, C. B. Eom, and T. W. Noh, "Multilevel data storage

memory using deterministic polarization control," Adv. Mater. **24**, 402–406 (2012).
[48]C. M. Wang, J. F. Wang, S. Zhang, and T. R. Shrout, "Electromechanical properties of A-site (LiCe)-modified sodium bismuth titanate) ($Na_{0.5}Bi_{4.5}Ti_4O_{15}$) piezoelectric ceramics at elevated temperature," J. Appl. Phys. **105**(9), 094110 (2009).
[49]N. Nukaga, K. Ishikawa, and H. Funakubo, "Growth of epitaxial $SrBi_2Ta_2O_9$ thin films by metalorganic chemical vapor deposition," Jpn. J. Appl. Phys., Part 1 **38**, 5428 (1999).
[50]A. Z. Simões, M. A. Ramirez, C. S. Riccardi, E. Longo, and J. A. Varela, "Ferroelectric characteristics of $SrBi_4Ti_4O_{15}$ thin films grown on Pt/Ti/SiO_2/Si substrates by the soft chemical method," Mater. Lett. **60**, 2020–2023 (2006).
[51]Y. Shimakawa, Y. Kubo, Y. Tauchi, T. Kamiyam, H. Asano, and F. Izumi, "Doping effect on the dielectric property in bismuth titanate," Appl. Phys. Lett. **77**(1), 2749 (2000).
[52]T. C. Chen, T. Li, X. Zhang, and S. B. Desu, "Doping effect on the dielectric property in bismuth titanate," J. Mater. Res. **12**(6), 1569–1575 (1997).
[53]T. Jia, H. Kimura, Z. Cheng, and H. Zhao, "Ferroelectric and magnetic properties of Aurivillius $Bi_{m+1}Ti_3Fe_{m-3}O_{3m+3}$ thin films," J. Vac. Sci. Technol. A **33**(6), 060605 (2015).
[54]Y. Yan, M. M. Al-Jassim, Z. Xu, X. Lu, D. Viehland, M. Payne, and S. J. Pennycook, "Structure determination of a planar defect in $SrBi_2Ta_2O_9$," Appl. Phys. Lett. **75**(13), 1961–1963 (1999).
[55]M. D. Maeder, D. Damjanovic, and N. Setter, "Lead free piezoelectric materials," J. Electroceram. **13**(1), 385–392 (2004).
[56]A. Chanthbouala, A. Crassous, V. Garcia, K. Bouzehouane, S. Fusil, X. Moya, J. Allibe, B. Dlubak, J. Grollier, S. Xavier, C. Deranlot, A. Moshar, R. Proksch, N. L. D. Mathur, M. Bibes, and A. Barthélémy, "Solid-state memories based on ferroelectric tunnel junctions," Nat. Nanotechnol. **7**, 101–104 (2012).
[57]D. S. Sohn, W. X. Xianyu, W. I. Lee, I. Lee, and I. Chung, "Ferroelectric $SrBi_4Ti_4O_{15}$ thin films with high polarization grown on an IrO_2 layer," Appl. Phys. Lett. **79**, 3672 (2001).
[58]M. Wuttig and N. Yamada, "Phase-change materials for rewriteable data storage," Nat. Mater. **6**, 824–832 (2007).
[59]A. V. Kolobov, P. Fons, A. I. Frenkel, A. L. Ankudinov, J. Tominaga, and T. Uruga, "Understanding the phase-change mechanism of rewritable optical media," Nat. Mater. **3**, 703–708 (2004).
[60]A. Onodera, K. Yoshio, C. C. Myint, S. Kojima, H. Yamashita, and T. Takama, "Ferroelectric instability and dimensionality in Bi-layered perovskites and thin films," Jpn. J. Appl. Phys., Part 1 **38**(9B), 5683–5685 (1999).
[61]Q. Q. Zhang, S. J. Gross, S. Tadigadapa, T. N. Jackson, F. T. Djuth, and S. TrolierMcKinstry, "Lead zirconate titanate films for d33 mode cantilever actuators," Sens. Actuators, A. **105**, 91–97 (2003).
[62]N. Hu, C. Lu, Z. Xia, R. Xiong, P. Fang, J. Shi, and J. Liu, "Multiferroicity and magnetoelectric coupling in $TbMnO_3$ thin films," ACS. Appl. Mater. Interfaces **7**(48), 26603–26607 (2015).
[63]S. Amiri and H. Shokrollahi, "Magnetic and structural properties of RE doped Co-ferrite (REåNd, Eu, and Gd) nano-particles synthesized by co-precipitation," J. Magn. Magn. Mater. **345**, 18–23 (2013).
[64]D. Caruntu, G. Caruntu, and C. J. O'Conno, "Magnetic properties of variable-sized Fe_3O_4 nanoparticles synthesized from non-aqueous homogeneous solutions of polyols," J. Phys. D: Appl. Phys. **40**, 5801–5809 (2007).
[65]M. A. Khan, M. J. Rehman, K. Mahmood, I. Alic, M. N. Akhtar, G. Murtazae, I. Shakir, and M. F. Warsi, "Impacts of Tb substitution at cobalt site on structural, morphological and magnetic properties of cobalt ferrites synthesized via double sintering method," Ceram. Int. **41**(2), 2286–2293 (2015).
[66]Y. Shimakawa, M. Azuma, and N. Ichikawa, "Multiferroic compounds with double-perovskite structures," Materials **4**, 153–168 (2011).
[67]K. Amanuma, T. Hase, and Y. Miyasaka, "Preparation and ferroelectric properties of $SrBi_2Ta_2O_9$ thin films," Appl. Phys. Lett. **66**, 221 (1995).
[68]R. Guo, L. You, Y. Zhou, Z. S. Lim, X. Zou, L. Chen, R. Ramesh, and J. Wang, "Non-volatile memory based on the ferroelectric photovoltaic effect," Nat. Commun. **4**, 1–5 (2013).
[69]A. Z. Simoes, A. H. M. Gonzalez, C. S. Riccardi, E. C. Souza, F. Moura, M. A. Zaghete, E. Longo, and J. A. Varela, "Ferroelectric and dielectric properties of lanthanum-modified bismuth titanate thin films obtained by the polymeric precursor method," J. Electroceram. **13**, 65–70 (2004).